Ag NANOCLUSTERS SUPPORTED ON TiO_2/GO WITH ENHANCED CATALYTIC ACTIVITY FOR THE PHOTOCATALYTIC OZONATION OF RR195 DYE

Received: 21-05-2025

Lê Hà Giang[1,2*], Phạm Thị Thu Trang[1], Dương Anh Thanh[1], Đào Ngọc Nhiệm[2,3], Trần Quang Vinh[1], Quản Thị Thu Trang[1]

[1]Institute of Chemistry, Vietnam Academy of Science and Technology
[2]Graduate University of Science and Technology, Vietnam Academy of Science and Technology
[3]Institute of Material Science, Vietnam Academy of Science and Technology
**E-mail:giangnasa86@gmail.com*

TÓM TẮT

CÁC HẠT NANOCLUSTER Ag ĐƯỢC PHÂN TÁN TRÊN CHẤT NỀN TiO_2/GO VỚI HOẠT TÍNH XÚC TÁC NÂNG CAO CHO QUÁ TRÌNH OZON HÓA QUANG XÚC TÁC THUỐC NHUỘM RR195

Lần đầu tiên hạt nanocluster Ag (Ag NCs) được phân lập và lắng đọng đơn lớp trên các thanh nano TiO_2 pha tạp graphene oxit (GO) bằng phương pháp cấy nguyên tử. Lượng tải Ag NCs (0,36 mol) với kích thước trung bình 5,17 nm trên vật liệu TiO_2/GO (TG) thúc đẩy quá trình dịch chuyển bước sóng hấp thụ ánh sáng sang vùng khả kiến (450 nm) đồng thời hạn chế quá trình tái tổ hợp e^-/h^+ và tăng cường độ dẫn điện từ đó giúp vật liệu nano compozit 3 thành phần chứa Ag NCs, TiO_2 và GO (ATG) thể hiện hiệu suất quang xúc tác và ozon hóa xúc tác (PCO) đều cao hơn so với TG. Kết quả cho thấy hằng số tốc độ phản ứng bậc 1 (k_{vis}) trong quá trình quang xúc tác phân hủy RR195 trên hệ ATG đạt 0,029 phút^{-1} và cao gấp 1,5 lần so với TG (0,0183 phút^{-1}), tương ứng. Ngoài ra, quá trình PCO cho thấy sự ưu việt hơn quá trình quang xúc tác đơn lẻ do sự tương tác hiệp đồng của quang xúc tác và O_3 đem lại. Giá trị k_{vis} của quá trình PCO trên hệ xúc tác ATG đạt 0,253 phút^{-1} cao gấp 9 lần k_{vis} của quá trình quang xúc tác (0,029 phút^{-1}). Kết quả này được cho là do sự có mặt dồi dào của các gốc oxy hóa (ROS) như $\bullet O_2^-$, $\bullet OH$ và h^+ được sinh ra thông qua các phản ứng dây chuyền xảy ra trong quá trình phản ứng. Đặc biệt, $\bullet OH$ là tác nhân chính trong quá trình PCO giúp tăng hiệu suất quá trình khoáng hóa (TOC) RR195 đạt 80,2% trên hệ xúc tác ATG và cao hơn so với TG (73,9%). Công trình này làm sáng tỏ việc thiết kế và chuẩn bị các hạt Ag NCs trong các hệ xúc tác trên cơ sở GO giúp tăng cường phân hủy các chất ô nhiễm hữu cơ bền vững một cách triệt để nhất.

Từ khóa: *Ống nano TiO_2, Graphen oxit, Thuốc nhuộm RR195, Ozon hóa quang xúc tác,*

1. INTRODUCTION

The acceleration of industry in the era of Industry 4.0 has contributed to improved living standards for humans; however, it has also led to a rise in pollution-related issues, such as dyes and pesticides [1]. The red dye RR195, which belongs to the azo family and contains the organic group –N=N– and the sulfonic acid group (–SO_3–), has been widely used in the textile industry. The degradation of RR195 in the environment generates aromatic amines, which were carcinogenic and pose significant health risks to humans [2]. Therefore, the removal of RR195 from wastewater was essential. Advanced oxidation processes (AOPs) were recommended as a preferred method for this purpose, owing to their high potential for total organic carbon (TOC) removal [1]. However, using AOPs alone might lead to

incomplete mineralization or only moderate efficiency [1]. The photocatalytic ozonation (PCO) method using TiO_2 showed great potential in degrading persistent organic compounds [3, 4]. As was known, ozone (O_3) was an electron-deficient molecule with Lewis acid and base characteristics. Consequently, O_3 is typically adsorbed on the surface of catalysts via acid-base interactions, after which it could capture electrons generated from the catalyst to form reactive oxygen species (ROS). The activation efficiency of O_3 on the catalyst surface was highly dependent on the electronic structure of the catalyst [3].

Nanoclusters were small assemblies of atoms or molecules, typically ranging from 1 nm to 100 nm, occupying an intermediate state between single atoms and nanoparticles. They were easier to fabricate than single atoms and exhibited unique physical and chemical properties that differ significouldtly from nanoparticles [5]. Due to their ability to exist in multiple oxidation states, nanoclusters enhanced the efficiency of redox cycles and facilitated better electron transfer than single atoms and nanoparticles [5]. Yiqing Li and colleagues successfully synthesized a TiO_2 catalyst doped with 2.5% CuO_x nanoclusters (1 nm), which increased the reaction rate by 2.2 - 4.0 times compwered to the individual use of TiO_2 or O_3. The results showed that defects in CuO_x promoted rapid adsorption and activation of O_3, thereby accelerating the reaction rate [6]. According to N. Sobana, the separation of photoinduced electrons in TiO_2 could be enhanced by the presence of Ag compounds during the photocatalytic process [7]. Moreover, the Ag component was an effective catalyst for decomposing O_3 into reactive radicals [3].

In our previous work, we synthesized a TiO_2 catalyst doped with graphene oxide (GO). The TiO_2/GO (TG) catalyst exhibited significouldtly enhanced photocatalytic degradation and PCO removal efficiency compwered to pure TiO_2. However, the TOC mineralization efficiency reached only 74% after 60 minutes of RR195 degradation [8]. Therefore, to further enhance the oxidative degradation of RR195, we incorporated silver nanoclusters (Ag NCs) into the TiO_2/GO catalyst system (TG), aiming to create a new catalyst system ATG, which was expected to exhibit superior catalytic performance compwered to TG in both photocatalytic and PCO processes under visible light in the wavelength range of 400 - 600 nm.

2. METHODOLOGY

2.1. Chemical

Reactive Red 195 (RR195) dye, $AgNO_3$, HCl, NaOH, and TiO_2-P25 were all sourced from China and used directly without further purification. High-purity nitrogen gas (N_2, 99.99%) and oxygen gas (O_2, 99.99%) were supplied by Venmer Company, Vietnam. All synthesis and treatment processes were carried out using single-distilled water.

2.2. Atomic Implantation-Assisted Synthesis of the ATG Catalyst

The TG catalyst containing 5 wt.% GO was synthesized according to the procedure reported in our previous work [8]. Subsequently, 1.0 gram of the TG catalyst was weighed and introduced into a tube furnace system comprising two separate chambers divided by a quartz membrane [9]. A specific amount of $AgNO_3$ (equivalent to 2 wt.% Ag^o relative to TG) was introduced into the chamber opposite the one containing the TG catalyst. Nitrogen gas was flowed through

the system from the Ag-containing chamber toward the TG-containing chamber, then directed through a NaOH trap to neutralize any toxic gases before environmental release. The tube furnace was then heated to 350 ^{o}C at a ramping rate of 10 ^{o}C/minute (min.). and maintained at this temperature for 1 hour. At this temperature, the Ag precursors form nanoclusters that anchor onto defect sites on the TG surface, resulting in the formation of the ATG catalyst. The final product was then cooled to room temperature and stored in a sealed container.

2.3. Characterization of Catalysts

The TG and ATG catalysts were characterized using various analytical techniques. X-ray diffraction (XRD) analysis was conducted on a D8 Advance diffractometer (Germany) using Cu Kα radiation (λ = 1.5406 Å) over a 2θ range of 1^{o}–70^{o}. Transmission electron microscopy (TEM) was performed using a JEO 2100 (Japan). Brunauer–Emmett–Teller (BET) surface werea measurements were obtained using a Tristar Plus II instrument (Micromeritics, USA). The optical properties of the catalysts were evaluated using UV-Vis diffuse reflectance spectroscopy (DRS) and photoluminescence (PL) spectroscopy, as well as electrochemical impedance spectroscopy (EIS) [10]. Electron paramagnetic resonance (EPR) spectroscopy was employed to detect the presence of reactive oxygen species (ROS) during the reactions [10]. For the reuse cycles, after each reaction, the photocatalyst was thoroughly washed with water and ethanol, then dried at 100 ^{o}C for 6 hours.

2.4. Reaction system and procedures

Removal efficiency of Photocatalytic and PCO Processes on the Batch System for 200 mL as Described in the Previous Publication [8]. Catalyst concentration: 0.05 - 0.5 g/L, RR195 concentration: 50 mg/L, O_3 flow rate: 0.5 - 1.5 L/min., and pH varied from 3 to 10 to find the optimal conditions.

Total organic carbon measurements were carried out using a Shimadzu (Japan). The removal efficiency (RE%) was calculated using the equation 1:

$$RE\% = (1 - C/C_o) \times 100 = (1 - TOC/TOC_o) \times 100 \quad \text{(Eq. 1)}$$

The pseudo-first-order kinetic constant (k_{vis}) was determined according to the method reported in the literature [10].

3. RESULTS AND DISCUSSION

3.1. Morphological Characterization of Catalysts

The XRD patterns of TG and ATG catalysts (Figure 1a) exhibited diffraction peaks at 2θ = 25.3^{o}, 38.0^{o}, 48.0^{o}, 53.9^{o}, 55.1^{o}, 62.9^{o}, 69.0^{o}, 70.1^{o}, and 75.4^{o}, which could be indexed to the (101), (004), (200), (105), (211), (204), (116), (220), and (215) crystal planes of anatase TiO_2 (JCPDS 21-1272), respectively [3]. The peak at 2θ ≈ 9.6^{o}, typically attributed to GO, was no longer observed, indicating that most of the GO was reduced to RGO. The RGO peak near 2θ ≈ 25^{o} was also not visible due to overlap with the (101) plane of anatase TiO_2 at 25.3^{o} [4]. The similarity in XRD peak positions between TG and ATG suggestsed that Ag nanoparticles formed and anchored onto the TiO_2 nanorods without disrupting the TiO_2 crystal structure [4].

The nitrogen adsorption–desorption isotherms shown in Figure 1b indicated that TG and ATG exhibited type IV isotherms with H3-type hysteresis loops, typical of slit-like mesopores, likely formed by the stacking of Ag-TiO_2 nanorods on the GO surface. The specific

surface wereas of TG and ATG were higher than those of pure TiO_2, confirming the contribution of the GO substrate in the composite materials [8]. The surface area of ATG was slightly lower than that of TG, likely due to the Ag nanoclusters (Ag NCs) partially covering the TiO_2 nanorod surfaces. This was also reflected in the pore diameter distributions: TG exhibited pores ranging from 20 - 27 nm, while ATG showed slightly smaller pores of 20 - 21 nm.

The TEM image of TG (Figure 1c) revealed the characteristic wrinkled and layered two-dimensional structure of GO, which facilitated the uniform dispersion of TiO_2 nanorods across its surface [4]. The TiO_2 nanotubes exhibited lengths of several hundred nanometers and diameters of approximately 7 - 8.5 nm, consistent with previous reports [11]. The TEM image of ATG (Figure 1d) showed Ag nanoclusters (average size ≈ 5.17 nm) anchored on both the TiO_2 nanotube and GO layers. This observation aligned with BET data indicating an increased pore diameter of ≈ 6 nm, suggesting monolayer deposition of Ag on the TiO_2 nanotubes.

The XPS analysis confirmed the atomic composition of ATG as $Ti_{14.66}O_{51.37}C_{32.71}Ag_{0.36}$, with Ag accounting for approximately 1.99 wt%, which closely matched the theoretical value. XPS analysis of $Ag3d_{3/2}$ and $Ag3d_{5/2}$ revealed that silver primarily existed in the metallic state (Ag^o), with a small fraction oxidized to Ag^+ due to Ag–O–Ti interactions (Figure S1). This confirmed the successful deposition of Ag^0 nanoparticles on the TiO_2 surface and partial doping of Ag^+ into the TiO_2 lattice. These results highlighted the effectiveness of the atomic implantation method in achieving uniform nanocluster distribution, limiting aggregation, enhancing surface plasmon resonance (SPR), and reducing e^-/h^+ recombination via Ag^+ induced lattice defects, thereby boosting catalytic performance.

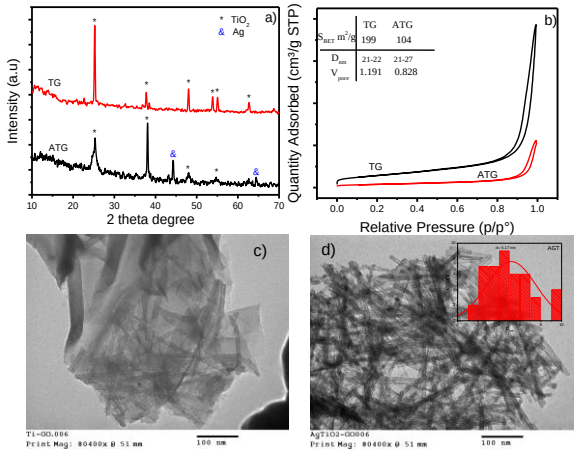

Figure 1. XRD patterns (a), BET isotherms (b), and TEM images (c, d) of TG and ATG catalysts

3.2. Optical Properties of Catalysts

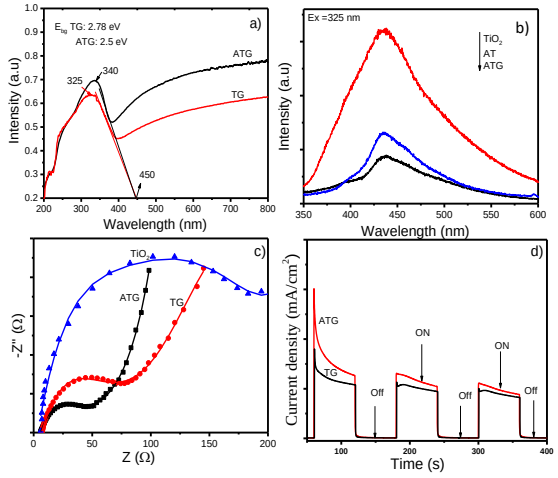

Figure 2. DRS spectra (a), PL spectra (b), EIS characteristics (Nyquist plots) (c), and time-dependent photocurrent responses (d) of TG and ATG catalysts.

The DRS spectra evaluating the optical absorption properties of TG and ATG were presented in Figure 2a. Pristine TiO_2 typically absorbed light with wavelengths below 390 nm [12]. However, introducting of Ag NCs and GO resulted in a redshift of the absorption edge for TG and ATG samples, extending to around 450 nm,

indicating enhanced light-harvesting capabilities. The absorption peak shifted from 325 nm (TG) to 340 nm (ATG), which was attributed to the surface plasmon resonance effect of the Ag NCs [12]. The optical bandgap energies (E_{bg}) of TG and ATG were estimated using Tauc plots for indirect bandgap semiconductors, by plotting $(\alpha h\nu)^{1/2}$ versus photon energy ($E = h\nu$). The resulting E_{bg} values were 2.78 eV for TG and 2.50 eV for ATG, respectively.

The PL spectra of TG and ATG were recorded to investigate the recombination behavior of photogenerated e^-/h^+ pairs and were shown in Figure 2b. A lower PL intensity indicated more effective electron trapping or transfer, while a higher intensity corresponded to faster e^-/h^+ recombination. Compared to pure TiO_2, both TG and ATG exhibited significantly reduced PL intensities, confirming that both GO and Ag NCs act as electron sank or transferred media, effectively suppressing the recombination of e^- /h^+ pairs in the ATG composite [12].

The EIS diagrams for TiO_2, TG, and ATG were presented in Figure 2c, providing insight into the interfacial charge separation and transport processes. The semicircle diameters in the Nyquist plots followed the ATG < TG < TiO_2 trend, indicating a substantial reduction in charge transfer resistance and improved charge mobility. These results confirmed that integrating Ag, TiO_2, and GO into a ternary heterostructure enhances interfacial charge transfer and, consequently, the photocatalytic performance [13].

Figure 2d presented the time-dependent photocurrent response of TG and ATG under UV light. In the absence of light, the photocurrent density of both samples approached zero. Upon illumination, the photocurrent density of ATG was significantly higher than that of TG. This result demonstrated the enhanced photoelectrochemical activity of ATG due to the incorporation of Ag NCs, which facilitated efficient charge separation and transport [13].

3.4. Photocatalytic degradation and Photocatalytic ozonation

The photocatalytic and PCO processes for TG and ATG in the degradation of RR195 dye were illustrated in Figure 3. As shown, the degradation rate and RE% of ATG were significantly higher than those of TG. Figure 3a indicated that TG exhibited a greater adsorption capacity for RR195 than ATG, likely due to its larger specific surface area. The adsorption equilibrium reached approximately 20% after 30 minutes in the dark. During the photocatalytic process, the k_{vis} for ATG reached 0.029 $min.^{-1}$, which was 1.5 times higher than that of TG (0.0183 $min.^{-1}$). After 120 minutes of light irradiation, the RE% of ATG and TG were 91% and 85%, respectively.

Upon light irradiation, the TiO_2 particles in the ATG composite were excited, and photogenerated electrons from the valence band could be rapidly transferred through GO and onto Ag NCs. This cascade transfer suppressed e^- /h^+ recombination, effectively prolonging the lifetime of charge carriers. On the surface of Ag NCs, these electrons reduced adsorbed O_2 to form superoxide radicals ($\bullet O_2^-$), highly reactive species capable of oxidizing RR195 anions [13, 14]. EPR analysis shown in Figure 3b confirmed that $\bullet O_2^-$ radicals were the dominant reactive species during the photocatalytic process. The $\bullet O_2^-$ signal intensity for ATG was higher than that of TG under the same irradiation time, in agreement with earlier analyses indicating enhanced photocatalytic efficiency of ATG.

Compared to photocatalysis alone, PCO performance was significantly enhanced for TG and ATG catalysts. Indeed, the degradation rate in the PCO process was approximately ten times higher than in the photocatalytic process alone, with k_{vis} values of 0.184 $min.^{-1}$ for TG and 0.253 $min.^{-1}$ for ATG (Figure 3c). The RE% reaches 97.76% after just 20 minutes of reaction. The TOC removal efficiency ranged from 41% to 50% at 20 minutes, and reached 75% - 80% after 60 minutes, demonstrating the synergistic effect between photocatalysis and ozonation [1, 3].

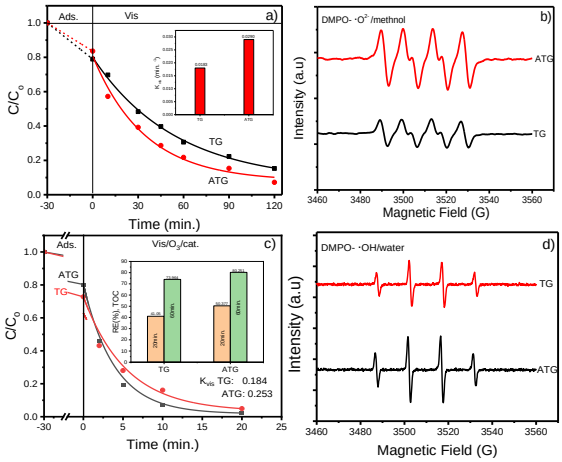

Figure 3. Photocatalytic degradation (a), PCO process (b), EPR spectra during photocatalysis (c), PCO (d) of RR195 dye using TG and ATG catalysts.

In the PCO process, electron-rich functional groups on the surface of ATG and TG acted as catalytic sites, facilitating dissolved ozone adsorption and donating electrons to O_3. This promotes its rapid decomposition and generates a higher concentration of reactive species such as $•O_2^-$, hydroxyl radicals (•OH), and photogenerated holes (h^+), which played key roles in RR195 degradation [1]. The EPR spectra in Figure 3d confirmed the prominent formation of •OH radicals during PCO, highlighting their crucial role. Since the reaction rate constant of •OH was higher than that of $•O_2^-$, the PCO process was more effective than standalone photocatalysis [10]. This also implied that the PCO system using ATG could efficiently mineralize persistent organic pollutants. From the analytical results obtained, we proposed a mechanism for the photocatalytic ozonation process under visible light irradiation, which was described in the supplementary and Figure S2.

3.5. Influence of factors for RR195 degradation

Figure 4a showed the impact of catalyst dosage on the PCO process using ATG. As the catalyst concentration increased from 0.05 g/L to 0.5 g/L, the k_{vis} increased to 0.253 $min.^{-1}$, then slightly decreased to 0.245 $min.^{-1}$. This was attributed to the enhanced active sites for O_3 adsorption, which increased the ROS and thus accelerated the reaction rate [1]. However, when the catalyst dosage was excessively increased, the reaction solution became turbid, hindering light penetration to the catalysts and thereby reducing the reaction rate [8].

Figure 4b illustrated the strong influence of initial pH on the PCO process. At pH values below 6, the reaction rate increased to 0.516 $min.^{-1}$, but dropped significantly to 0.159 $min.^{-1}$ at pH 10. As was known, RR195 dissociated in water, forming anions, and the pH at the point of zero charge (pH_{zpc}) of TiO_2-based composite materials typically fell around 6.3 [15]. Under conditions where pH < pH_{zpc}, the surface of ATG became positively charged, favoring the adsorption of RR195 anions. At higher pH values, electrostatic repulsion became unfavorable for RR195 adsorption. Additionally, when pH > 9, the concentration of •OH radicals increased, causing H_2O_2 in the solution to react with •OH to form perhydroxyl ($•HO_2$) radicals, which had a lower oxidation potential than

•OH and O_3, thus reducing the RR195 degradation rate [16]. The reaction rate constant kvis was higher at pH 3 than at pH 6, but we selected pH 6 for practical applications for this study.

Figure 4c showed the effect of O_3 flow rate on the reaction rate. As the O_3 flow rate increased from 0.5 L/min. to 1.5 L/min., the reaction rate constant increased from 0.195 $min.^{-1}$ to 0.357 $min.^{-1}$, respectively. With increased O_3 flow, the O_3 concentration in the solution rised, enabling more efficient trapping of photogenerated electrons from the ATG irradiation, leading to the generation of more ROS and enhancing the degradation of RR195 [1]. However, at an O_3 flow rate of 1.5 L/min., excessive foam formation led to catalyst loss, so an O_3 flow rate of 1.0 L/min. was chosen for the study.

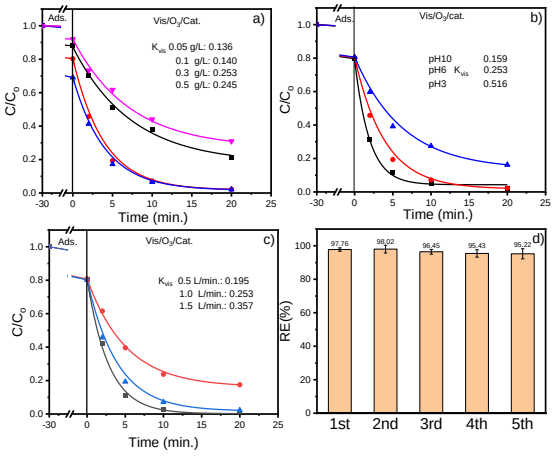

Figure 4. Effects of reaction conditions on the PCO process using ATG: catalyst dosage (a); pH (b); O_3 flow rate (c); catalyst reuse (d).

Under the optimal conditions for this study: pH 6, catalyst concentration of 0.3 g/L, O_3 flow rate of 1 L/min., and a reaction time of 20 minutes, the RE% reached 97.76%, and the TOC removal efficiency was 80.25%. After five reaction cycles, the RE% only decreased by 2.5%, indicating that ATG possesses excellent stability and catalytic performance for the PCO degradation of RR195 (Figure 4d). Moreover, the comparative data in Table S1, highlighting the performance of various catalysts alongside the ATG catalyst developed in this study, demonstrated that ATG was a highly efficient system and a promising coulddidate for the effective removal of persistent organic pollutants from aqueous environments.

4. CONCLUSION

The ATG nanocomposite was successfully synthesized using hydrothermal and atomic implantation methods. The presence of small Ag NCs (5.17 nm) and high GO layers enhanced the photocatalytic and photocatalytic ozonation efficiencies. XRD, BET, PL, and EIS analyses confirmed the surface plasmon resonance of Ag NCs, the increased surface werea due to the contribution of the GO layer, which helps prevent charge recombination, and the enhanced conductivity. As a result, the ATG exhibited superior photocatalytic performance compwered to TG. The reaction rate constant of ATG was 1.5 times higher than that of TG in the photocatalytic process under visible light irradiation for 120 minutes.

Moreover, the PCO process performed better than the standalone photocatalytic process on both ATG and TG systems. The reaction rate constant for PCO on ATG (0.253 $min.^{-1}$) was nine times higher than that for the photocatalytic process (0.029 $min.^{-1}$). This result was attributed to the synergistic interaction between photocatalysis and O_3, which generated more ROS and accelerated the reaction rate. The ATG catalyst demonstrated excellent stability after five reaction cycles, indicating its potential for the degradation of persistent organic compounds via the PCO process.

REFERENCES

[1] Liao G, et al., (2024). Efficient treatment of surfactant containing wastewater by photocatalytic ozonation with $BiPO_4$ nanorods. *Chemosphere*, **346**, 140594.

[2] Luo L, Huang H, Heng Y, Shi R, Wang W, Yang B, and Zhong C, (2022). Hierarchical-pore UiO-66-NH_2 xerogel with turned mesopore size for highly efficient organic pollutants removal. *Journal of Colloid and Interface Science*, **628**, 705-716.

[3] Ling Y, Liao G, Xie Y, Yin J, Huang J, Feng W, and Li L, (2016). Coupling photocatalysis with ozonation for enhanced degradation of Atenolol by Ag-TiO_2 micro-tube. *Journal of Photochemistry and Photobiology A: Chemistry*, **329**, 280-286.

[4] Ayoubi-Feiz B, Mashhadizadeh M H, and Sheydaei M, (2019). Degradation of diazinon by new hybrid nanocomposites N-TiO_2/Graphene/Au and N-TiO_2/Graphene/Ag using visible light photo-electro catalysis and photo-electro catalytic ozonation: Optimization and comparative study by Taguchi method. *Separation and Purification Technology*, **211**, 704-714.

[5] Yan H, Xiang H, Liu J, Cheng R, Ye Y, Han Y, and Yao C, (2022). The Factors Dictating Properties of Atomically Precise Metal Nanocluster Electrocatalysts. *Small*, **18(23)**, 2200812.

[6] Li Y, Fu M, Zhang X, He C, Chen D, Xiong Y, Guo L, and Tian S, (2023). Enhanced catalytic ozonation performance by CuO_x nanoclusters/TiO_2 nanotube and an insight into the catalytic mechanism. *Journal of Colloid and Interface Science*, **651**, 589-601.

[7] Sobana N, Muruganadham M, and Swaminathan M, (2006). Nano-Ag particles doped TiO_2 for efficient photodegradation of Direct azo dyes. *Journal of Molecular Catalysis A: Chemical*, **258(1)**, 124-132.

[8] Lê Hà Giang P T T T, Dương Anh Thanh, Đào Ngọc Nhiệm, Trần Quang Vinh, Quản Thị Thu Trang, (2024). Effect of graphene oxide loading on the catalytic activity of TiO_2/MGO in photocatalytic ozonation of RR195 dye. *Tạp chí Phân tích Hóa, Lý và Sinh học*, **4**, 34-41.

[9] Nguyen T T, Le G H, Le C H, Nguyen M B, Quan T T T, Pham T T T, and Vu T A, (2018). Atomic implantation synthesis of Fe-Cu/SBA-15 nanocomposite as a heterogeneous Fenton-like catalyst for enhanced degradation of DDT. *Materials Research Express*, **5(11)**, 115005.

[10] Le G H, Thanh D A, Pham T T T, Tran Q V, Dao N N, Nguyen K T, and Quan T T T, (2025). Synthesis of Z-scheme $Ag_4V_2O_7$/Ag_3VO_4/GO nanocomposites for photocatalytic degradation of DDT under visible light. *RSC Advances*, **15(9)**, 7078-7089.

[11] Liu X, Yan R, Zhu J, Zhang J, and Liu X, (2015). Growing TiO_2 nanotubes on graphene nanoplatelets and applying the nanonanocomposite as scaffold of electrochemical tyrosinase biosensor. *Sensors and Actuators B: Chemical*, **209**, 328-335.

[12] Sim L C, Leong K H, Ibrahim S, and Saravanan P, (2014). Graphene oxide and Ag engulfed TiO_2 nanotube arrays for enhanced electron mobility and visible-light-driven photocatalytic performance. *Journal of Materials Chemistry A*, **2(15)**, 5315-5322.

[13] Serikov T M, Kayumova A S, Baltabekov A S, Ilyina L F, and Zhanbirbayeva P A, (2023). Photocatalytic Activity of Nanocomposites Based on Titania Nanorods and Nanotubes Doped with Ag and Reduced Graphene Oxide

Nanoparticles. *Nanobiotechnology Reports*, **18(2)**, 207-215.

[14] Zhang L, Ni C, Jiu H, Xie C, Yan J, and Qi G, (2017). One-pot synthesis of Ag-TiO_2/reduced graphene oxide nanocomposite for high performance of adsorption and photocatalysis. *Ceramics International*, **43(7)**, 5450-5456.

[15] Ali M H H, Al-Afify A D, and Goher M E, (2018). Preparation and characterization of graphene – TiO_2 nanocomposite for enhanced photodegradation of Rhodamine-B dye. *Egyptian Journal of Aquatic Research*, **44(4)**, 263-270.

[16] Hafeez A, Javed F, Fazal T, Shezad N, Amjad U-e-S, Rehman M S u, and Rehman F, (2021). Intensification of ozone generation and degradation of azo dye in non-thermal hybrid corona-DBD plasma micro-reactor. *Chemical Engineering and Processing - Process Intensification*, **159**, 108205.